

# A fresh look into pulsating PG1159 stars

Alfred Gautschy

Astronomisches Institut der Universität Basel, Venusstr. 7, CH-4102 Binningen, Switzerland

[the date of receipt and acceptance should be inserted later]

**Abstract.** To improve the understanding of the pulsational instabilities of some of the PG1159-type pre-white dwarfs we performed detailed stability analyses on helium star evolutionary models. With the canonical chemical compositions, pulsational instabilities were encountered for all stellar masses considered (0.57, 0.63, 0.7  $M_{\odot}$ ). The blue boundary agrees satisfactorily with observations. The red edge, on the other hand, is found to extend lower temperatures than presently admitted by observers. The dependence of the pulsational instabilities on helium or even hydrogen abundance in the stellar envelopes is less stringent than emphasized hitherto. In particular, we found pulsationally unstable  $g$  modes for model stellar envelopes which are representative for HS2324+3944, a newly discovered PG1159-star with a hydrogen abundance  $X \approx 0.2$  and being pulsating.

**Key words:** Stars: oscillations – stars: white dwarfs – stars: interiors

## 1. Introduction

The hottest known stars are in their post-AGB phase shortly before settling onto the cooling sequence of white dwarfs. Corresponding stellar evolutionary tracks show a pronounced ‘knee’ joining the evolution at almost constant luminosity with one at almost constant radius (cf. Fig. 2). Spectroscopic observations show that some of the objects in that domain of the Hertzsprung-Russell (HR) diagram have high abundances of helium, carbon and oxygen. Characteristic properties of their spectra are the absence of hydrogen but strong helium, carbon, and oxygen features (see e.g. Dreizler et al. 1995). Such stars are named after the prototype PG1159-035. About 50 % of the 32 known PG1159 stars are surrounded by planetary nebulae and can be considered as direct descendents of recent leavers of the AGB. Those without indications of associated nebulosities cannot be attributed unambiguously an evolutionary state.

Some of the PG1159 stars are photometrically variable with periods ranging from 10 to about 30 minutes

(also termed GW Vir or DOV stars, we will use the first name in the following). Nine variable stars of this class are known by now. The high-luminosity members of the class show typically about four times longer periods than those being close to the white dwarfs’ cooling tracks. The longer-period PG1159 stars are typically variable central stars of planetary nebulae and are referred to as PNNVs or variable CSPNe in the literature. Since there are also cooler variable central stars it might be appropriate to stress that we consider here the *hot* PNNVs with  $T_{\text{eff}}$  around  $10^5$  K. In this paper we will not further distinguish between the high- and low-luminosity branch of the evolution track. Hence, in the discussions of the mode physics it is of no further importance if a GW Vir variable is surrounded by a planetary nebula or not. For aspects of evolution and/or population statistics of the instability region the very presence of a planetary nebula might of course help to discern between different scenarios.

The GW Vir variability is attributed to the overstability of low-degree, high-order gravity ( $g$ ) modes. The observed frequency spectra are very rich – i.e. many modes are excited simultaneously – and they are used for seismological analyses with considerable success (e.g. Kawaler & Bradley 1994). Based on the data of a WET observing campaign, the power spectrum of the variability of PG1159-035 itself, for example, allowed the resolution of 125 individual frequency peaks (Winget et al. 1991). For seismological studies, excitation physics of the pulsation modes is irrelevant. The results from adiabatic oscillation calculations – neutrally stable oscillations modes – serve to identify the observed peaks in the power spectra. Irregularities in the distribution of the oscillation frequencies provide a tool to probe aspects of the internal structure of the oscillators. The main objective of seismological studies is to constrain the stratification of the stellar envelopes and of course the accurate measurement of global stellar parameters which are not directly accessible otherwise.

The physical origin of the pulsational instability of GW Vir-type was addressed in the middle of the eighties by Starrfield et al. (1984, 1985). They identified partial K-shell ionization of carbon and/or oxygen as the destabilizing agent. Due to the rather weak opacity bump pro-

duced by this ionization processes, even minor contamination of the stellar matter by elements other than C and O are considered as effectively destroying pulsational instabilities. In particular, H and He were banished from the excitation region which were assumed to be made up of mixtures of C and O only in the studies of Starrfield et al. (1984, 1985). A marginal instability region, shortly before the knee, was obtained the a mass fraction of 0.1 of He in Stanghellini et al. (1991). A higher helium abundance could not account for *any* hot variables of GW Vir type.



**Fig. 1.** The observed distribution of some of the PG1159-035 stars on the  $T_{\text{eff}} - \log g$  plane. Solid dots show the spectroscopic calibration of photometrically stable stars. The white circles indicate the GW Vir variables and the hot, variable central stars of planetary nebulae (hot CSPNe). The solid lines derive from our stellar evolution calculations of helium stars which were performed for this study. The grey area covers the observationally defined instability domain of PG1159 stars.

Since the GW Vir variables are few a reliable observational determination of the borders of the instability region is difficult and probably still rather unreliable. An attempt was presented recently by Werner et al. (1995). The grey area in Fig. 1 approximating the instability region is based on Werner & Rauch’s data; theirs, however continues to lower  $\log g$  values which are not of interest for us since the most massive star we consider has  $0.7M_{\odot}$ .

Recently, Saio (1996) reviewed the pulsation properties of hydrogen-deficient stars. Therein he also dealt with GW Vir variables and hot, variable CSPNe. Using the new generation opacity data (the OPAL brand in his case) he encountered pulsational instabilities for chemical compositions which were not found when using the old opacity tables. Saio’s computations suggest that the previously stringent chemical composition constraints for pulsational instabilities need to be relaxed. He presented a period –  $T_{\text{eff}}$  diagram which shows convincing overlap with observational data.

A major unresolved problem is posed by the observation that a PG1159 star located within the instability region, lets say on the  $\log T_{\text{eff}} - \log g$  plane, does not compulsively imply its variability. Based on the presently known PG1159 stars, only about half of the population encountered in the instability domain pulsates. The dilemma intensifies as we know of spectroscopic twins of which one is variable and the other stable (Werner et al. 1991).

This paper presents a nonradial, nonadiabatic survey of low-degree g-modes in GW Vir-like stars using the new OPAL opacity data for the radiative opacities. Partially, it can be considered as supporting the recent results of Saio (1996). The modeling methods are described in Sections 2 and 3. We emphasize aspects of stellar and mode physics and to some degree the influence of the chemical composi-

tion mainly on a qualitative level rather than trying to fit particular observations in Sects. 4 and 6. One exception is the star HS2324+3944 which was recently discovered to be a PG1159 star which shows measurable amounts hydrogen in its spectrum *and* additionally it is a pulsating variable. Section 5 deals with our modeling of this object.

## 2. Construction of the PG1159 models

The stellar background models on which the stability analyses were performed relied on results from stellar evolution computations. The nonradial oscillation analyses were hence performed on complete stellar models. The finite-difference scheme used solves the structure/evolution equations from the center to the photosphere of the models. The physical processes accounted for in the code are the same as described in the paper of Gautschy et al. (1995). In particular, we point out that He, C, *and* O ionization are accounted for in the equation of state (EoS). All regions of the stellar interior are treated with the identical formulation of the EOS to avoid discontinuities in thermodynamical quantities at switching points of the formulations. Convection was dealt with in the standard MLT approach with a mixing length of 1.5 pressure scale height. For the very hot stars in which we are interested in here the particular formulation of convective energy transport should not be very crucial. Opacity data were taken from the freely accessible CO enhanced OPAL repository (in its 1992 version) at Livermore ( $\kappa_{\text{table}}$ ). At very high temperatures, above  $10^8$  K, the tables were frequently not broad enough in the  $R$  variable to accommodate the stellar interiors. In such high-temperature domains we extended the tables with approximations by analytical formulae as described in Gautschy et al. (1996)( $\kappa_{\text{analyt.}}$ ). To avoid jumps in the Rosseland mean and its partial derivatives we defined an ad-hoc overlap region in temperature over which we switch linearly, according to  $\theta \cdot \kappa_{\text{table}} + (1 - \theta) \cdot \kappa_{\text{analyt.}}$ , between the two approaches. The transition width spanned usually about  $10^6$  K. To make best use of the OPAL data we also implemented their interpolation code (`cotrin`) interpolating within a single opacity table as well as between different chemical compositions for a fixed amount of hydrogen. We included nuclear burning of He to C, O, and Ne. Energy losses by neutrinos were included with the fits of Munakata et al. (1985). Elemental diffusion in the strong gravitational field building up after passing the knee was not included in the calculations.

Our model series started as homogeneous helium main-sequence stars with a composition compatible with observed surface abundances in PG1159 stars. Except if noted otherwise, we used  $X = 0$ ,  $Y = 0.38$ ,  $C = 0.4$ ,  $O = 0.2$ . Figure 2 shows the evolutionary tracks of the three stellar masses ( $0.57, 0.63$  and  $0.7M_{\odot}$ ) which were evolved for the purposes of this study. The chemically homogeneous helium zero-age main-sequence models were

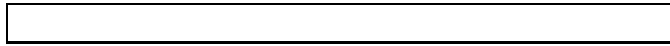


**Fig. 2.** Loci of the initially chemically homogeneous helium stars with  $0.57$ ,  $0.63$ , and  $0.70M_{\odot}$  on the HR diagram. Stability analyses were performed on models having passed their maximum luminosity. The internal structure of such models resembles that of models coming directly from the AGB and having lost their H-rich envelope by some mechanism. The overlaid heavy line indicates regimes where pulsationally overstable  $\ell = 1$  modes were found.

followed as far as possible through the core and shell helium burning. During the He-shell burning episode they approach the post-AGB tracks of originally H-rich ‘canonical’ stellar models. By the time the effective temperature has risen to about  $10^5$  K the position of the He stars on the HR diagram and their interior structure is close to results from canonical stellar evolution. Therefore, we are confident that our He star models provide access to rather realistic structures for PG1159 stars to perform stability analyses on. Figure 1 indeed confirms that our evolutionary tracks (for phases after having passed the maximum luminosity) compare well with the tracks from standard stellar evolution when they cross the GW Vir instability domain (cf. Dreizler et al. 1995). The  $0.6M_{\odot}$  locus occurring on the  $\log g - T_{\text{eff}}$  plane of Fig. 1 is the result of early test computations and was not used for further nonradial oscillation analyses. Figure 2 shows the evolutionary tracks of the three stellar masses ( $0.57$ ,  $0.63$  and  $0.7M_{\odot}$ ) which were evolved for the purposes of this study. The more massive two sequences run out of the opacity tables at rather low temperatures already (a few times  $10^7$  K) shortly after the knee so that the computations were stopped at that point. The  $0.57M_{\odot}$  could be followed very far down the cooling track. We terminated its evolution calculations after it reached  $\log T_{\text{eff}} = 4.7$  at a luminosity of  $1.7L_{\odot}$ .

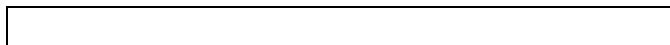


**Fig. 3.** Example of the chemical stratification of a  $0.7M_{\odot}$  model passing through the luminosity maximum shown in Fig. 1.

A representative spatial run of the chemical stratification of the PG1159 star models is displayed in Fig. 3. It corresponds to a model from the  $0.7M_{\odot}$  series around the luminosity maximum. The burning shell starts at about  $0.8M_{*}$ . Within about a tenth of the stellar mass helium is burned away. As evolution proceeds the burning shell propagates outward. Except for a translation, the functional form of the abundance profile does not change significantly. The same applies when considering different stellar masses.

### 3. Nonradial nonadiabatic oscillation treatment

The nonradial, nonadiabatic stellar oscillation code was the same as described in the paper of Gautschy et al. (1996). The nuclear terms were included here for the sake of completeness. As helium burning only was considered, equilibrium treatment of the  $\epsilon$ -mechanism was sufficient. The boundary conditions in the center are dictated by the regularity of the perturbations of the physical quantities. At the surface we assume that the Stefan-Boltzmann law for radiation obtains and full reflection of the waves as the mechanical boundary condition. Convection was always treated as being frozen-in, ie. the perturbation of the convective flux was assumed to be negligible. In most of the hot models the particular treatment of convection might be irrelevant due to its marginal contribution to the energy transport. A more detailed discussion of this point is postponed to Sect. 7. The eigenvalues  $\sigma = (\sigma_{\text{R}}, \sigma_{\text{I}})$ , where  $\sigma_{\text{R}}$  stands for the oscillation frequency and  $\sigma_{\text{I}}$  for the excitation/damping rate, are always expressed in units of  $\sqrt{3GM_{*}/R_{*}^3}$ .

### 4. Results from stability analyses

In this section we present the results of nonradial, nonadiabatic pulsation computations performed on  $0.7$ ,  $0.63$ , and  $0.57M_{\odot}$  evolutionary sequences. Each of the model series will be dealt with separately. We start by discussing the obtained *modal diagrams* (plot of period vs. some control parameter such as  $\log g$  or damping rate of a particular mode) and consider consequences therefrom. Mostly, the mode computations were restricted to  $\ell = 1$   $g$  modes.

We start with the most massive star sequence – the  $0.7M_{\odot}$  models. Figure 4 shows the variation of the periods of some of the  $\ell = 1$   $g$  modes as evolution proceeds. The star’s evolution is parameterized by its surface gravity which monotonically increases advancing evolutionary stage in the phases covered by us.

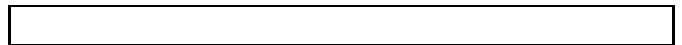


**Fig. 4.** Modal diagram of the lower-order,  $\ell = 1$   $g$  modes of the last part of the  $0.7M_{\odot}$  sequence. Top panel: Light lines trace the variation of the oscillation periods of particular overtones as the surface gravity changes during the evolution. Unstable regimes are marked by thick lines. The short period modes are separated by  $\Delta k = 1$  up to the mode pointed to with the appropriate error. The long-period modes are, as indicated with the other arrows, separated by  $\Delta k = 10$ . An exception is the mode with the asterisk. Its neighboring modes are separated by  $\Delta k = 5$ . Bottom panel: the variation of the imaginary parts of the modes. Due to the large range spanned by the imaginary parts the scaling is logarithmically for values much larger than  $10^{-8}$ .

The upper panel of Fig. 4 shows the variation of the periods of some  $g$  modes as the star evolves around the

knee. A particular radial order is traced by a thin line. Since we were dealing with high-order modes a small fraction only of the radial orders (denoted by  $k$ ) in the period domain of interest for GW Vir variables was followed. In this respect, the upper panel can be divided again. In the low-period domain – between about 50 and 200 s – we computed eigenvalues for every radial order. Above about 300 s – in the long-period regime – only every 10th radial order (region between the arrows originating from  $\Delta k = 10$  in Fig. 4) was followed. The only exception with  $\Delta k = 5$  to both sides is marked with an asterisk. For easier identification of the instability domains, the pulsationally unstable mode branches are traced with heavy lines. From the lower panel in Fig. 4 we see this to correspond to negative  $\sigma_I$  values in our sign convention of the eigenvalues. For better graphical presentation we appropriately scaled the large numerical range of the imaginary parts. Moduli of  $\sigma_I$  exceeding  $10^{-8}$  scale logarithmically in this choice of the ordinate. Smaller values behave essentially linear. The sign function allows to discern between stable and overstable oscillation modes.

The short-period domain in Fig. 4 shows sequences of avoided crossings occurring in low-order modes of low surface-gravity models. The avoided crossings appear in period as well as in the imaginary parts of the eigenfrequencies. A local analysis of the first model of the series shows that eigenmodes with periods below about 220 s have dual character. Deep in the interior they propagate as  $g$  modes and as  $p$  modes in the envelope. The less steep portions of the eigenmode branches which cause the avoided crossings reflect the different reaction on the stellar evolution of the  $p$ -mode propagation speed in the envelopes. Away from avoided crossings, the less steep branches correspond to modes which are dominated by the  $p$ -mode cavity. In accordance with a strong coupling with the envelope of the short-period modes early in our evolutionary phases they have, compared with core-dominated  $g$  modes, high damping rates which are induced by considerable radiative damping in the envelopes. Figure 4 shows imaginary parts as high as  $10^{-5}$  only. The largest  $\sigma_I$  values rise to about  $10^{-3}$ .

For a short phase of the evolution, one of the short-period modes turns weakly pulsationally unstable. The period ranges from 145 to 152 s. The excitation rate is very weak as can be seen in the lower panel of Fig. 4. We ensured its reality by re-iterating this mode several times with different accuracy bounds for the numerical scheme and with different start-guesses for the eigenvalue. Repeated convergence to this weak instability proved that we can confirm the pulsational instabilities at short periods which were also seen by Saio (1996, his Fig. 5). The instability is induced by the He-burning shell through the action of the  $\epsilon$ -mechanism. Only a very narrow period range and a very short evolutionary phase are prone to such instabilities. In the  $0.7M_\odot$  star models this leads to one radial order only which can be weakly destabilized at

$\ell = 1$ . The radial displacement eigenfunction of the unstable mode has 5 nodes within the  $g$ -mode cavity and none in the acoustic propagation region which it hardly touches anymore. The maximum growth rate of the nuclearly destabilized  $g$  mode amounts to an e-folding time of  $1.5 \cdot 10^3$  y. The star’s evolution through this instability phase takes about 10 times longer. This might be marginally sufficient for an  $\epsilon$ -destabilized mode to build up. In comparison with the long-period gmode instabilities, the instabilities effected by the  $\epsilon$ -mechanism appear to be hardly of relevance.

In the long-period domain, where modes have always pure  $g$ -mode character, pulsational instabilities occur for periods longer than 880 s (cf. Fig. 4). The higher the radial order of the modes the lower the surface gravity for which instability shows up. The locus of the mode marked with ‘\*’ has  $k = 45$ . It was inserted in the usual  $\Delta k = 10$  sequence to more accurately determine the low-period border of the instability region. Figure 4 shows a small fraction only of all the modes that are pulsationally unstable. We restricted the computation of overtones as high as necessary to find stable modes again to the first stellar model of the particular model sequence. The longest-period mode which was unstable in the  $0.7M_\odot$  sequence lies at about 7447 s. This is a truly remarkable range of simultaneously unstable radial orders. Since the Riccati method does not involve the simultaneous computation of the eigenfunctions when relaxing eigenfrequencies we estimate the range of radial orders covered by the asymptotic  $g$ -mode period separation formula. For the model at  $\log g = 5.94$ ,  $\log T_{\text{eff}} = 5.045$ , and  $\ell = 1$  we deduce about 200 modes to be simultaneously unstable. The return to stability of the very-high overtones appears rather abruptly. Over most of the unstable period range, the imaginary parts remain at  $\sigma_I = \mathcal{O}(10^{-6})$ .



**Fig. 5.** Same as Fig. 4 but for the  $0.63M_\odot$  series. The outlined numbers are locations where different spherical degrees were computed; they are discussed in Sect. 6. The horizontal line at  $\log g = 6.745$  indicates the position where period separations and the variation of the imaginary parts of eigensolutions of subsequent radial orders.

The models of the  $0.63M_\odot$  evolutionary track were processed similarly as those of the  $0.57M_\odot$  sequence. The resulting  $\ell = 1$  modal diagram is shown in Fig. 5. Only the modes relevant for the eventually uncovered instability region are shown. The modal analysis of the  $0.63M_\odot$  models is the most dense one – in terms of covered radial orders – of this project. The radial-order spacing between the displayed lines in the top panel of Fig. 5 are labeled.

As in the  $0.70M_\odot$  case, the instability region has an expressed finger-like shape pointing from low- $\log g$  and long periods to high- $\log g$  and short periods. The high- $\log g$

edge of the instability region occurs at about  $\log g = 6.85$ . The hottest point of the  $0.63M_{\odot}$  evolutionary track is encountered at  $\log g = 7.0$ . Hence, the instability domain terminates before  $0.63M_{\odot}$  stars start to dim their luminosities. Our computations showed no return to pulsational instability of the evolutionary models during their ‘downward’ evolution anymore (as indicated in Fig. 1).

Again, a large number of radial overtones remained overstable also in the earliest model of the sequence and extending again to very long periods. Therefore we stopped the tracking of particular radial orders around 5000 s. The very smooth and stretched ridge in  $\sigma_{\text{I}}$  is seen in Fig. 7’s lower panel. In contrast to classical pulsators such as Cepheids or RR Lyrae stars, a large number of radial overtones appear to be simultaneously favored for excitation. The highest-order  $\ell = 1$  mode which was found overstable at  $\log g = 5.83$  has a period of about 9500 s.

The locus of the  $k = 91$  dipole mode is marked in Fig. 5. This serves to count the radial orders of the other modes plotted and to emphasize the high order of excited modes. The number of nodes was counted in the displacement eigenfunction. This particular mode was chosen because it belongs to those modes with maximal instability in the  $0.63M_{\odot}$  sequence. We return to in Sect. 6.



**Fig. 6.** Same as Fig. 4 but for the  $0.57M_{\odot}$  series. The dashed horizontal line marks the hot-most point of the evolutionary knee. For higher surface gravities the star approaches the white dwarf cooling tracks.

The lowest-mass evolutionary sequence considered here had  $0.57M_{\odot}$ . The results from the nonadiabatic eigenanalyses for  $\ell = 1$  are shown in Fig. 6. In contrast to the before-mentioned sequences, here the instability domain extends beyond the knee into the cooling phase. Therefore we indicated the to highest effective temperature reached with a horizontal line at the appropriate  $\log g$  value. For economic reasons we restricted ourselves to a rather coarse coverage of the period domain. The low period range ( $\Pi \lesssim 800$  s) was scanned with  $\Delta k = 5$  until we reached that radial order which did not turn overstable during the evolutionary phase depicted in Figs. 1 or 2. At long periods we stopped the tracking of modes after the first model of the  $0.57M_{\odot}$  sequence turned pulsationally unstable. For the first model we searched the longest overstable mode which was found at about 5500 s.

The long-period ‘instability finger’ is also contained in Fig. 5. It merges, however, with a short-period instability domain which extends to low luminosities and hence late evolutionary stages. Periods as short as 300 s become overstable. The  $\ell = 1$   $g$  modes of the last model of the  $0.57M_{\odot}$  evolutionary sequence were all pulsationally stable again. Hence, the red edge on the low-luminosity branch lies at  $\log T_{\text{eff}} = 4.45$  and  $\log L/L_{\odot} = -0.1$ . In our computations

there is one radial order (the third longest) which becomes pulsationally overstable at high luminosities and again – after a phase of stability – at low luminosities.

The lower panel of Fig. 6 shows the variation of the imaginary parts of the eigenfrequencies. The high-luminosity part is smooth and looks very similar to the results of the more massive star sequences. The low-luminosity imaginary parts are, despite their comparable modulus, less smooth. This is not numerically caused. At low luminosities the transition from the He-rich envelope to the pure CO core is rather steep and as close to the surface as it can ever come. Therefore, the  $g$  modes are partially reflected at the composition transition such that trapping of modes could be expected. Such trapping of modes also shows up in the imaginary parts of the eigenfrequencies (cf. Gautschy et al. 1996) leading to the ‘bumpy’ appearance. We finally notice that the width of the instability with respect to radial orders is much narrower at low luminosities than on the high-luminosity branch. The envelope covering the short-period  $\sigma_{\text{I}}$  peaks in the lower panel of Fig. 6 crosses zero at a very steep angle at about 1000 s. This is much different from the behavior of the envelope of the  $\sigma_{\text{I}}$  curves in larger-mass sequences for which the long periods are unstable only on the high-luminosity branch of the evolutionary track.

## 5. The peculiar case of HS2324+3944

Dreizler et al. (1996) reported the discovery and spectroscopic analysis of the peculiar PG1159 star HS2324+3944. In contrast to the other members of this class it shows an atmospheric ratio (by number) of He to H of 0.5. Furthermore, HS2324 shows an unusual low oxygen abundance. In mass fractions, we adopt  $X=0.2$ ,  $Y=0.41$ ,  $C=0.37$ ,  $O=0.01$  (Werner, private communication). Recently, Silvotti (1995) provided first observational results indicating that HS2324 is a GW Vir-type variable with a dominant period of about 2140 s. According to previous nonradial stability analyses (e.g. Starrfield et al. 1984) any trace of hydrogen was considered poisoning pulsational instabilities.

The spectroscopic calibration places HS2324 at about  $\log g = 6.2$  and  $\log T_{\text{eff}} = 5.11$  (Dreizler et al. 1996). Based on the loci of our helium-star models in the  $\log g - \log T_{\text{eff}}$  plane, we assumed a stellar mass of  $0.63M_{\odot}$ , this is slightly larger than what Dreizler et al. proposed. We constructed stellar envelope models with homogeneous chemical composition adopting abundances as mentioned in the last paragraph. The integration starting at the stellar surfaces extended to the onset of significant hydrogen burning at about  $3 \times 10^7$  K.

The bottom panel of Fig. 7 clearly shows the decrease of the opacity in the envelope models with HS2324 composition when compared with the evolutionary helium star models. The opacity bump around  $\log T = 6.25$  appears



**Fig. 7.** Comparison of pulsationally interesting physical quantities between  $0.63M_{\odot}$  He star models (pg63 seq.) and envelope models for HS2324. The HS2324 models differ in their chemical composition, in particular the under-abundance in O compared with the evolutionary sequences. Top panel: logarithmic opacity derivative with respect to temperature at constant density. Bottom panel: spatial run of the logarithm of the opacity. The depth in the stellar envelopes is parameterized by the temperature.

to become narrower. Hence, pulsational driving is not expected to be significantly weakened by neither the existence of hydrogen nor the suppressed oxygen abundance. The  $\kappa_T$  slope in both stellar models (HS2324 envelope and evolutionary He-star) are comparable (cf. top panel of Fig. 7). Actually, the slope in the HS2324 model appears to be marginally steeper than in the full He-star model.

### 5.1. The pulsation properties of HS2324

As for the full helium-star models, we performed eigenanalyses on the envelope models for HS2324. The inner boundary of the envelope was treated as a reflective wall. This influences the period spacing between adjacent orders of the computed  $g$  modes only. In the cases considered the spacing was about five times larger than for full  $0.63M_{\odot}$  models with comparable effective temperature. The magnitude of the work integrals are not expected to be much different. Most of driving and damping occurs below  $\log T = 6.5$ . In particular the decisive contributions to stability or instability come from there. In HS2324 we miss some dissipation from the deep interior. The Brunt-Väisälä frequency achieves its maximum close to the center so that the eigenfunctions have there their most rapid spatial oscillations. From the full models we derive that only a few % of the total work is done in the deep interior. Our imaginary parts are hence expected to be marginally too large. The qualitative behavior is, however, believed to be correct.

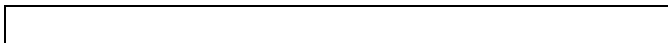


**Fig. 8.** Appropriately scaled imaginary parts of eigenfrequencies as a function of period of  $\ell = 1$   $g$  modes. The two curves show the results of two different choices of the stellar models'  $T_{\text{eff}}$  both at  $\log L/L_{\odot} = 3.16$ .

Figure 8 displays the imaginary parts of low-order  $\ell = 1$   $g$  modes for two different envelope models. Obviously it is possible – even with the considerable hydrogen admixture of 20 % in mass – to obtain pulsational instabilities for HS2324-like stellar envelopes. Figure 8 shows that the destabilized period range depends markedly on the choice of effective temperature. Based on the results

for  $\ell = 1$  and the observed period of the variability we tend to favor a temperature closer to  $\log T_{\text{eff}} = 5.07$  which is lower – but still within the limits of uncertainty – than suggested by Dreizler et al. (1996).

As Fig. 8 clearly shows, the period domain over which dipole modes become pulsationally unstable is much narrower in the HS2324 models than in the hydrogen-free and oxygen-rich helium-star models. The excitation rates are comparable in both cases. Hence, it is not at all surprising if pulsations develop – as they do in GW Vir variables – in HS2324-like objects. The frequency spectrum must be expected to be poorer, though.

## 6. Discussion

In the following we take a closer look at the properties of the computed eigensolutions and the physical properties of the driving behind GW Vir-type instability.



**Fig. 9.** Work integral and normalized radial displacement of the nonadiabatic eigensolution for  $k = 91, \ell = 1$  of the  $0.63M_{\odot}$  model at  $\log g = 6.43$ . This mode belongs to the most unstable ones encountered. Blow-ups of the central behaviors in displacement and contributions to the work integral are shown as small insets.

The high quality of the nonadiabatic eigensolutions which was achieved in this study can be seen in Fig. 9. The top panel displays  $\rho r^2(|\xi_r| + \ell(\ell+1)|\xi_h|) \propto e_{\text{kin}}$  which corresponds – up to a normalization – to  $dE_{\text{kin}}/dr$  where  $E_{\text{kin}}$  stands for the total kinetic energy of an oscillation mode. The global run of  $e_{\text{kin}}$  shows the large weight of the deep interior for the kinetic energy of the mode. This behavior is characteristic of all  $g$  modes in our models. The expressed central concentration of  $e_{\text{kin}}$  leads to large values of  $E_{\text{kin}}$  which, in a quasi-adiabatic sense, explain the small values of  $\sigma_I$ . Even if the positive and negative parts of the work integral do not nearly cancel. The local depression in the amplitude of  $e_{\text{kin}}$  around  $\log P = 21.5$  coincides with the inner edge of the shell-burning region and the occurring abundance bump in carbon (which is also visible in Fig. 3). Mode trapping can be associated with such features. For a recent study of ZZ Ceti stars touching this aspect see Gautschy et al. (1996). The effect is so weak, though, that it is not of much relevance for observational properties of GW Vir stars. Mode trapping will be addressed further down in more detail.

The bottom panel of Fig. 9 displays the total work done by the particular oscillation mode. The dominant driving and damping contributions lie between  $\log P = 10$  and 14. A more detailed physical discussion follows. The rapid oscillations of the eigenmodes deep in the star lead to a small damping contribution of the total work only.



**Fig. 10.** Eigensolution components and stellar envelope properties of the same model and the same mode as used for Fig. 9. To concentrate on the main driving and damping regions of the oscillations, we restrict the plot to temperatures below  $\log T = 7.5$ .

A blow-up of the deep interior shown in the inlet in the lowest panel quantifies this statement.

Figure 10 shows selected quantities from nonadiabatic nonradial analysis of the dipole mode  $k = 91$  as well as from the stellar envelope structure of the underlying model (at  $\log g = 6.34$  of the  $0.63M_{\odot}$  sequence). This figure is the basis of a more detailed physical discussion of mode excitation.

The top panel of Fig. 10 depicts the superficial regions of the radial component of the displacement eigenfunction. It demonstrates that most of the spatial oscillations of the eigenfunctions are not significantly involved in the excitation/damping of the mode. The differential work  $dW/dr$  is seen to be significant in the range  $5.8 < \log T < 6.8$ . Mode-driving is restricted to the range between 5.8 and 6.4 in  $\log T$  which is in accordance with the opacity bump which reaches a local maximum around  $\log T = 6.25$ . This feature which is due to the combined effects of L-shell transitions of Fe and K-shell transitions C, O, and Ne (cf. Seaton et al. 1994) was found to be slightly enhanced (about 20 %, Iglesias et al. 1992) in the new tabulations of stellar opacities (OPAL and OP). Mainly, however, its shape became more pronounced so that it stands out even more clear in a plot of  $\kappa_T = \partial \log \kappa / \partial \log T | \rho$ . Figure 7 demonstrates the influence of strongly reducing the oxygen abundance in the stellar matter. The opacity is globally decreased, the bump around  $\log T = 6.2$  decreases also. The sharpness of its ridge on the  $\log R - \log T$  plane is, however, hardly influenced. Therefore, the  $\kappa_T$  run is not very much affected by reducing the O abundance. From the spatial ionization structure of the stellar envelope used for Fig. 10 we see that partial K-shell ionization of carbon might contribute only in the outer parts of the envelope, at temperatures below  $10^6$  K. Mostly oxygen K-shell ionization and bound-bound transitions in Fe dominate the hotter, more important part of the work integral. We admit that the comparison of the EoS and the opacity data is not fully satisfactory. We were not able to use the OPAL EoS tables with our high C and O abundances for the discussion. Hence, we must rely on our simplified approach which is, hopefully, not too far from reality (cf. Gautschy et al. 1996).

The  $\kappa$ -effect consists of two terms which contribute to driving if

$$\frac{d}{dr} \left( \kappa_T + \frac{\kappa_{\rho}}{(\Gamma_3 - 1)} \right) > 0. \quad (1)$$



**Fig. 11.** Period separation and variation of imaginary parts of successive radial orders for the  $0.63M_{\odot}$  model at  $\log g = 6.745$  (indicated by the horizontal line in Fig. 5) for  $\ell = 1$ .



**Fig. 12.** Reaction of the imaginary parts of eigenvalues of selected  $0.63M_{\odot}$  models (outlined numbers in Fig. 5) on varying the spherical degree  $\ell$ .

From the panel in Fig. 10 which displays the second term in the bracket it is obvious that its gradient is small throughout the driving region and it contributes – if at all – in the low-temperature part only. Below  $10^6$  K,  $\Gamma_3 - 1$  drops noticeable only when the ionization stages O VIII and O IX are already considerably populated. At higher temperatures  $\Gamma_3 - 1$  is completely flat so that the first term of Eq. 1 controls the driving peak of the differential work.

The period separation and the variation of the imaginary parts as a function of successive radial orders of dipole modes of a selected  $0.63M_{\odot}$  model are shown in Fig. 11. This particular stellar model is close to the hottest point of the corresponding evolutionary track. Its position is indicated by a horizontal line in the modal diagram of Fig. 5. In the period range between 600 and 1200 s no obvious sign of mode trapping is visible. In particular, no trapping shows up in the imaginary parts (much in contrast to the way trappings appear in ZZ Ceti stars, cf. Gautschy et al. 1996). The oscillation-period separation ( $\Delta\Pi$ ) as a function of period shows small, seemingly uncorrelated variations on the level one second. The reason is either intrinsic or then reflects the achieved numerical accuracy. The asymptotic formula for low-degree, high-order modes predicts a  $\Delta\Pi \approx 23.7$  s which is in reasonable agreement with the full solutions. An averaged period-separation curve might possibly hint at a trapping cycle which would then, however, considerably exceed 600 s.

Figure 5 contains the numbers one to four in an outlined font. At these locations we investigated the dependence of the eigensolutions on varying the spherical degree  $\ell$ . Mathematically,  $\ell$  can be treated as a continuous variable which was done to generate Fig. 12. The imaginary parts resulting from such a variation are displayed in Fig. 12. Notice that in contrast to other plots of  $\sigma_I$  values, the ordinate has a linear scale. Except at location 2, dipole modes appear to be the most unstable ones. Only at the tip of the instability finger, i.e. at position 2, the marginal instability of dipole modes strengthens towards higher  $\ell$  values and achieves a maximum at about  $\ell = 2.4$ . From the observational point of view, we expect  $\ell = 1$  and  $\ell = 2$  modes to dominate the oscillation spectra.

## 7. Conclusions

We computed three sequences of helium stellar models (at  $0.57$ ,  $0.63$  and  $0.7M_{\odot}$  which passed through  $\log g - T_{\text{eff}}$  the domain which is also populated by GW Vir variables. A large number of mostly dipole oscillation modes were investigated towards their stability properties with a fully nonadiabatic pulsation code.

GW Vir-like pulsations are driven, as we know for a while already (e.g. Starrfield et al. 1984) by the  $\kappa$ -mechanism of partial ionization of oxygen and carbon. Our Fig. 10 shows the associated opacity bump which peaks around  $1.7 \cdot 10^6$  K and which is somewhat enhanced in the new opacity tables (OP: Seaton et al. 1994, OPAL: Iglesias et al. 1992) compared with old data. It appears that not only detailed atomic physics of partial K-shell ionization in carbon, oxygen, and neon are relevant but that spin – orbit coupling of L-shell transitions in iron increases the sharpness of the bump feature additionally. The literature was, in our opinion, never very specific on the particular roles, carbon and oxygen played in the *final* picture. According to our EoS, which is not the same as that used in the opacity computations, it should be mainly partial ionization of the K-shell of oxygen which influences the driving of the pulsations. The last ionization level of carbon can only influence the low temperature flank of the driving regime but it cannot dominate the driving. This conclusion should of course be tested at some point in detail with consistent EoS and opacity data. As seen in the case of HS2324, carbon and oxygen abundances do not yet fully determine the problem. For the new variable HS2324, we assumed the oxygen abundance by mass to be as low as 0.01 and hydrogen to make up 20 % in mass. We still found pulsational instabilities. The domain of overstable modes was, though, much narrower than in the case of ‘canonical’ GW Vir compositions. Nevertheless, we conclude that the stringent composition requirements which were put forth hitherto (e.g. Starrfield et al. 1985, Stanghellini 1991) seem no longer to obtain with the new opacity data. Together with the  $\kappa$ -mechanism the  $\gamma$ -mechanism is frequently brought into play to explain GW Vir variability. The  $\gamma$ -mechanism is connected with the spatial variation of  $\Gamma_3 - 1$  in the second term of eq. 1. In the case of the GW Vir models, though, the K-shell ionization region of carbon and oxygen reduces  $\Gamma_3$  only marginally. In our pulsationally overstable models, maximum driving occurs at depths of the last partial ionization stage of oxygen for which  $\Gamma_3$  remains essentially constant. The second term of eq. (1) was shown as the third panel from below of Fig. 10. From this we conclude that the  $\gamma$ -effect is not effective for the action of the  $\kappa$ -mechanism in the GW Vir variables – an unusual situation in the theory of pulsating variable stars.

The instability region for dipole modes is shown with heavy lines in Fig. 2. When translated onto the  $\log T_{\text{eff}} - \log g$  plane, we find reasonable agreement of the blue edge

with observations. As already found in older studies (e.g. Stanghellini et al. 1991), the computed red edge occurs at much lower temperatures than what observations suggest. The  $0.57M_{\odot}$  models for which this applies in our study show only very weak convection zones close to the surface. A considerable leak of pulsation energy is therefore not likely to occur with an improved convection-pulsation coupling in our models. To introduce more efficient convection we would have to change the MLT prescription or at least assume a mixing-length parameter which is larger than ours which was chosen to be  $\alpha_{\text{MLT}} = 1.5$  pressure scale heights.

Furthermore, the longest periods which we found to be unstable significantly exceed the longest observed ones (around 2000 s). Lower stellar masses tended to have longer unstable periods. The longest period which we encountered has about 9500 s and belongs to the  $0.57M_{\odot}$  sequence. We saw that dissipation in the deep interior is only marginal compared to the contributions in the temperature range  $5.8 < \log T < 6.5$ . (cf. Fig. 10). Therefore, we expect the low-temperature region and the run of relevant components of the eigensolution therein to be decisive for the stability property rather than centermost parts of the stars with their very short spatial wavelengths of the eigenfunctions.



**Fig. 13.** Period – effective temperature diagram for the  $\ell = 1$  modes of the  $0.57M_{\odot}$  model sequence. As before, pulsationally unstable modes are shown with thick lines. For comparison, the two cool GW Vir stars PG2131+066 and PG0122+200 are overlaid with a bar spanning the observed period domain and indicating the  $T_{\text{eff}}$  uncertainty in the other direction.

In Fig. 13 we overlaid the observed oscillation period-range and the spectroscopic temperature calibrations of the cool GW Vir variables PG2131+066 and PG0122+200 on the same oscillation data as displayed in Fig. 6. We are interested in how well they fit into the theoretically determined unstable period domain of the  $0.57M_{\odot}$  sequence. We refer to the  $0.57M_{\odot}$  sequence since this is the only of our sequences which shows unstable oscillation modes at sufficiently low effective temperatures. We notice that a significantly smaller period range is observed than what the computations suggest. O’Brien et al. (1996) adopted a period spacing of 21.2 s for PG0122+200. This is smaller than the 24.1 s from our models. Increasing the stellar mass helps to reduce the discrepancy. Saio’s (1996) computations showed that the ‘blue edges’ of the  $g$ -mode instability regions along the white dwarfs’ cooling tracks are a function of mass. Increasing the stellar mass shifts the blue edge to lower effective temperatures and hence lower luminosities ( $\log T_{\text{eff}} = 5.08$  for  $0.58M_{\odot}$  and  $\log T_{\text{eff}} = 5.04$  for  $0.60M_{\odot}$ ). Based on the available data we cannot yet accurately estimate an upper limit of the mass of PG0122+200.



However, the hotter the star actually is the lower is this upper mass limit to guarantee consistency with the very existence of  $g$ -mode pulsations.

For none of our models could we find mode-trapping cycles (cf. the particular case of the  $0.63M_{\odot}$  model) that were of relevance for observed properties in GW Vir variables. The non-smooth run of  $\sigma_1$  at low luminosities of  $0.57M_{\odot}$ -sequence models marks trapping at the composition transition of the extinguishing He shell. Due to the large depth of this composition transition, the possible trapping length is much too long to be compatible with observational evidence. Hence, elemental diffusion is a necessary ingredient to interpret observed unequal period separations.

We still have to live with the enigma of seeing about as many stable as pulsating stars in the GW Vir instability domain. This problem is even somewhat aggravated by the results of this study since the particularities of the chemical composition are not necessarily as stringent as believed before. It is conceivable that the heavy element abundance in these objects has a stronger effect than believed up to now. If the iron-abundance is low enough, at least in the driving region, then driving might be reduced considerably even if carbon and oxygen abundances are PG1159-like. From the point of view of stellar evolution theory, mode trapping might prove to be a discriminant to distinguish between *first-passers* (on their first passage to the cooling track) and *late shell flashers*. For first passers at high enough luminosity or low enough surface gravity sedimentation by pressure diffusion might not have been very effective yet. This leads to a lack of  $\mu$ -barriers which can partially reflect and trap waves. Such stars are expected to show very regular period spacings which agree well with simple asymptotic formulae. On the other hand, low-luminosity stars or late shell flashers had enough time for He say, to float on top of carbon and oxygen. Even a shell flash need not necessarily destroy such a stratification if the star does not loop too far into the low- $T_{\text{eff}}$  domain. In such cases, the period separations should show cyclic depressions as observed or computed e.g. in PG1159 (Kawaler & Bradley 1994).

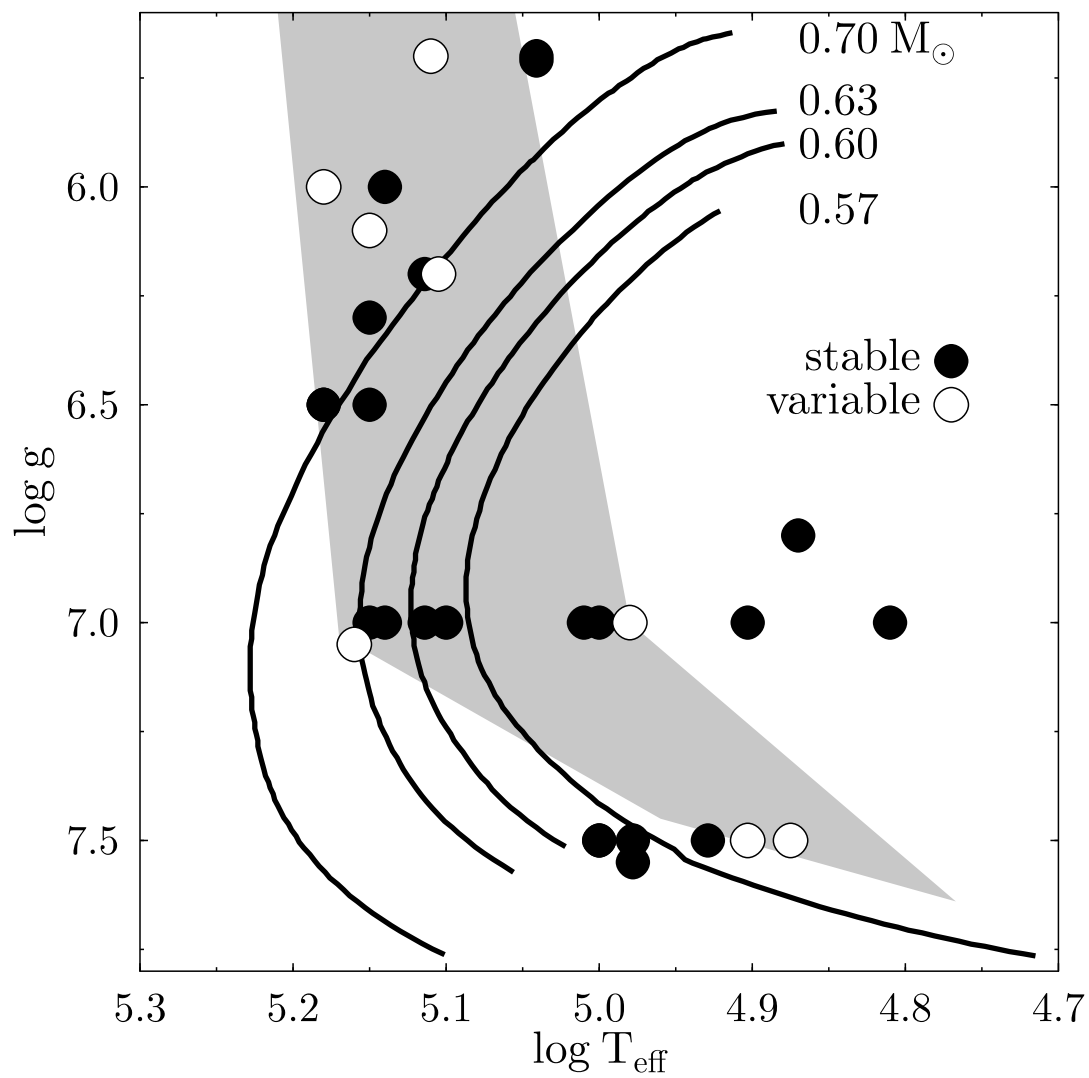
*Acknowledgements.* I am indebted to H. Saio for many helpful hints and critical comments throughout the project. K. Werner and S. Dreizler kindly informed me about

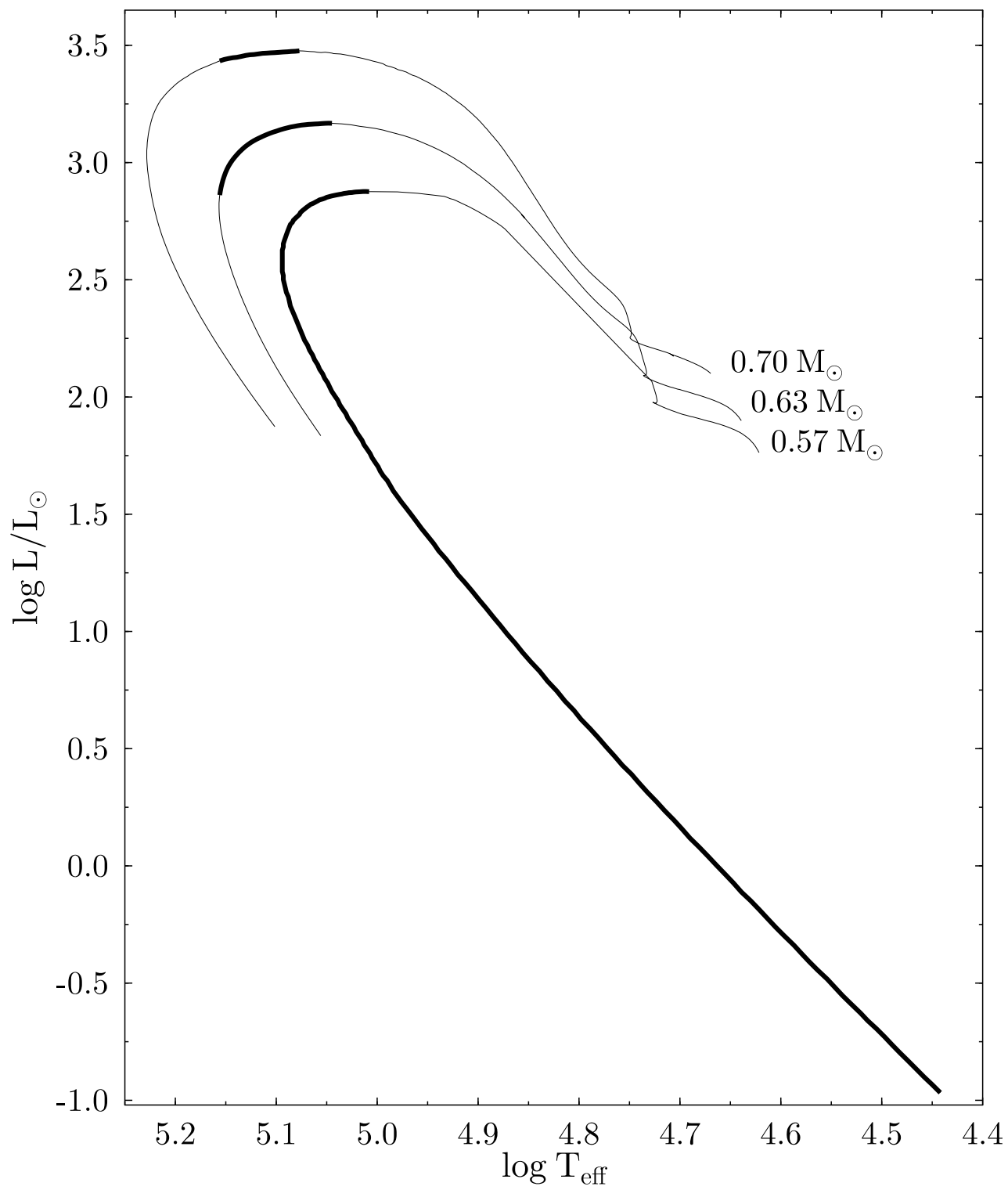
HS2324 properties prior to their publication. The Swiss National Science Foundation provided financial support through a PROFIL2 fellowship which is gratefully acknowledged.

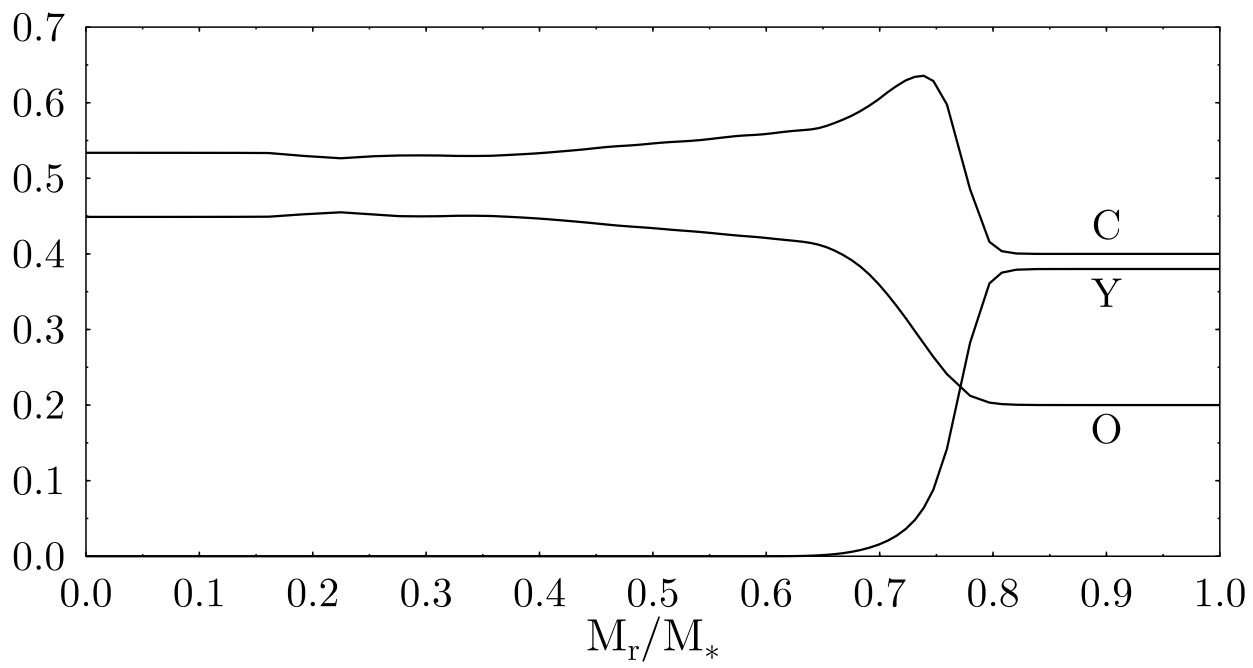
## References

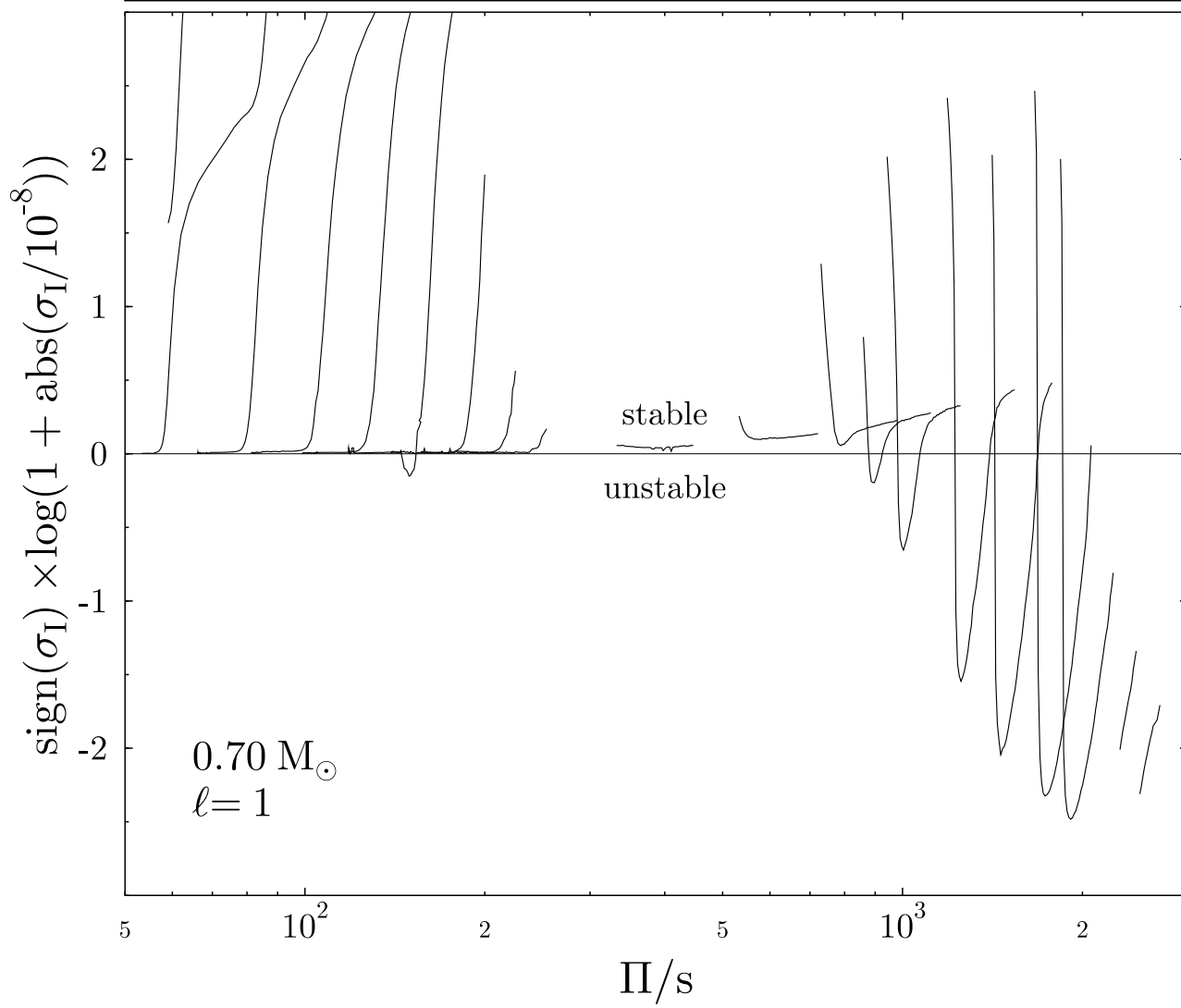
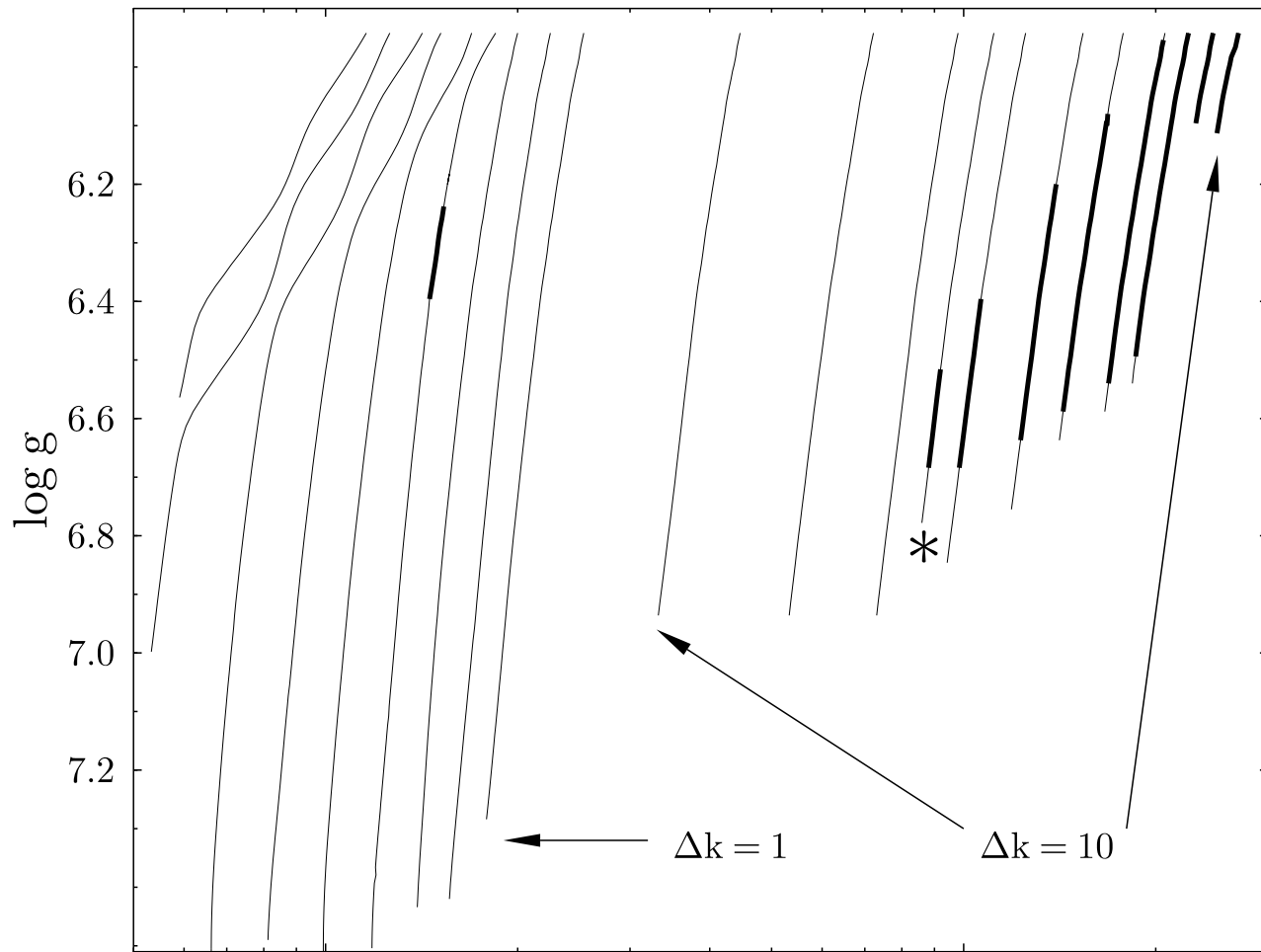
- Bergeron P., Wesemael F., Lamontagne R., Fontaine G., Saffer R.A., Allard N.F., 1995, ApJ 449, 258
- Dreizler S., Werner K., Heber U. 1995, in White Dwarfs, Lecture Notes in Physics 443, eds. D. Koester and K. Werner, Springer, p. 160
- Dreizler S., Werner K., Heber U., Engels D., 1996, A&A in press
- Gautschy A., Ludwig H.-G., Freytag G., 1996, A&A in press
- Iglesias C.A., Rogers F.J., Wilson B.G., 1992, ApJ 397, 717
- Kawaler S.D., Bradley P.A. 1994, ApJ 427, 415
- Munakata H., Kohyama Y., Itoh N. 1985, ApJ 296, 197; Erratum in ApJ 304, 580
- O'Brien M.S., Clemens J.C., Kawaler S.D., Benjamin T., 1996, preprint
- Silvotti R., 1995, IBVS 4265
- Saio H. 1996, in Hydrogen Deficient Stars, Proceedings of the Bamberg conference 1995, in press
- Seaton M.J., Yu Yan, Mihalas D., Pradhan K. 1994, MNRAS 266, 805
- Stanghellini L., Cox A.N., Starrfield S. 1991, ApJ 383, 766
- Starrfield S., Cox A.N., Kidman R.B., Pesnell W.D. 1984, ApJ 281, 800
- Starrfield S., Cox A.N., Kidman R.B., Pesnell W.D. 1985, ApJ, L23
- Werner K., Rauch T., Dreizler S., Heber U. 1995, in Astrophysical Applications of Stellar Pulsation, IAU Coll. 155, eds. R.S. Stobie and P.A. Whitelock, ASP Conf. Ser. Vol. 83, 96
- Werner K., Heber U., Hunger K. 1991, A&A 244, 437
- Winget D.E., Nather R.E., Clemens J.C., Provencal J., Kleinman S.J., et al. 1991, ApJ 378, 326

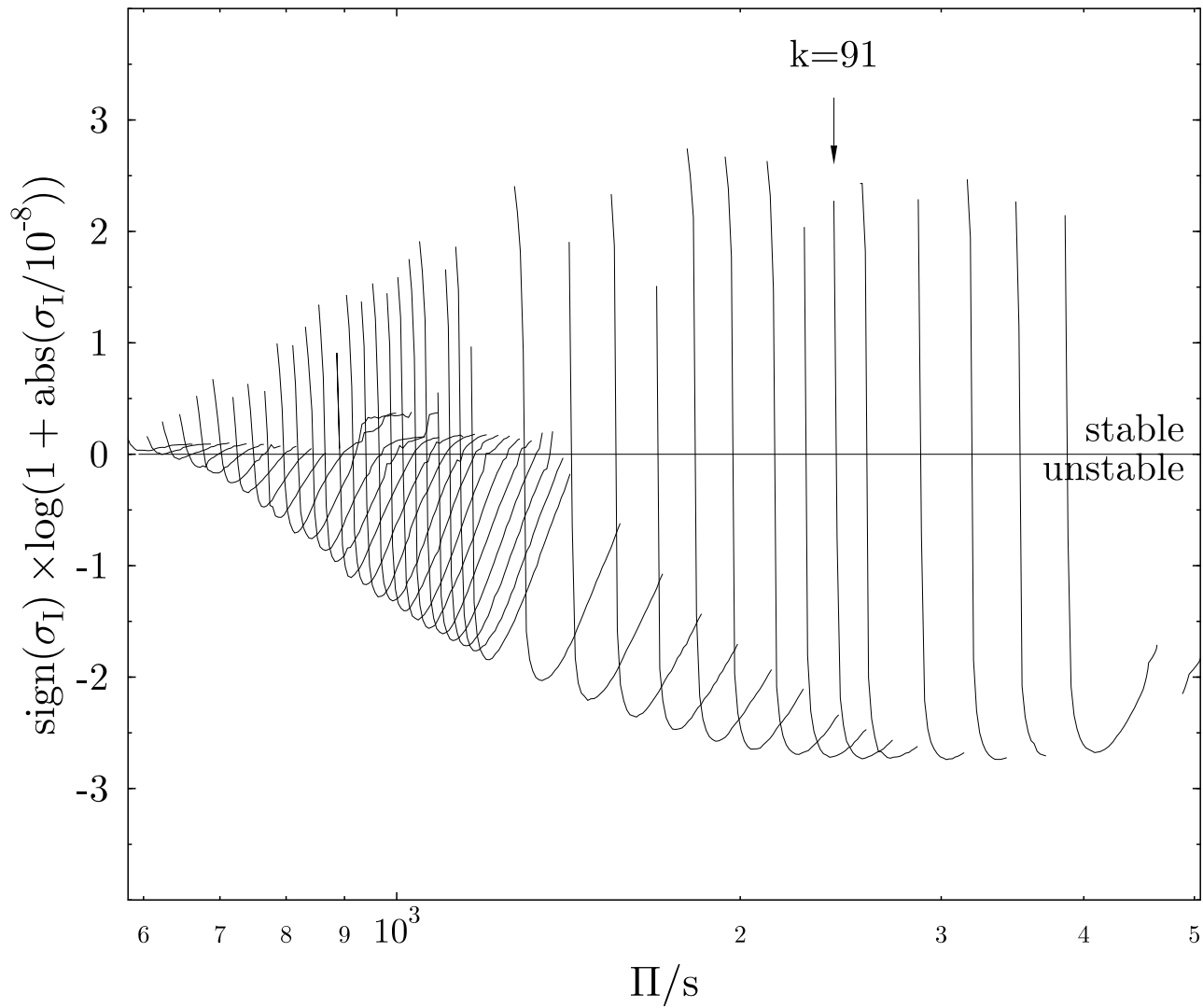
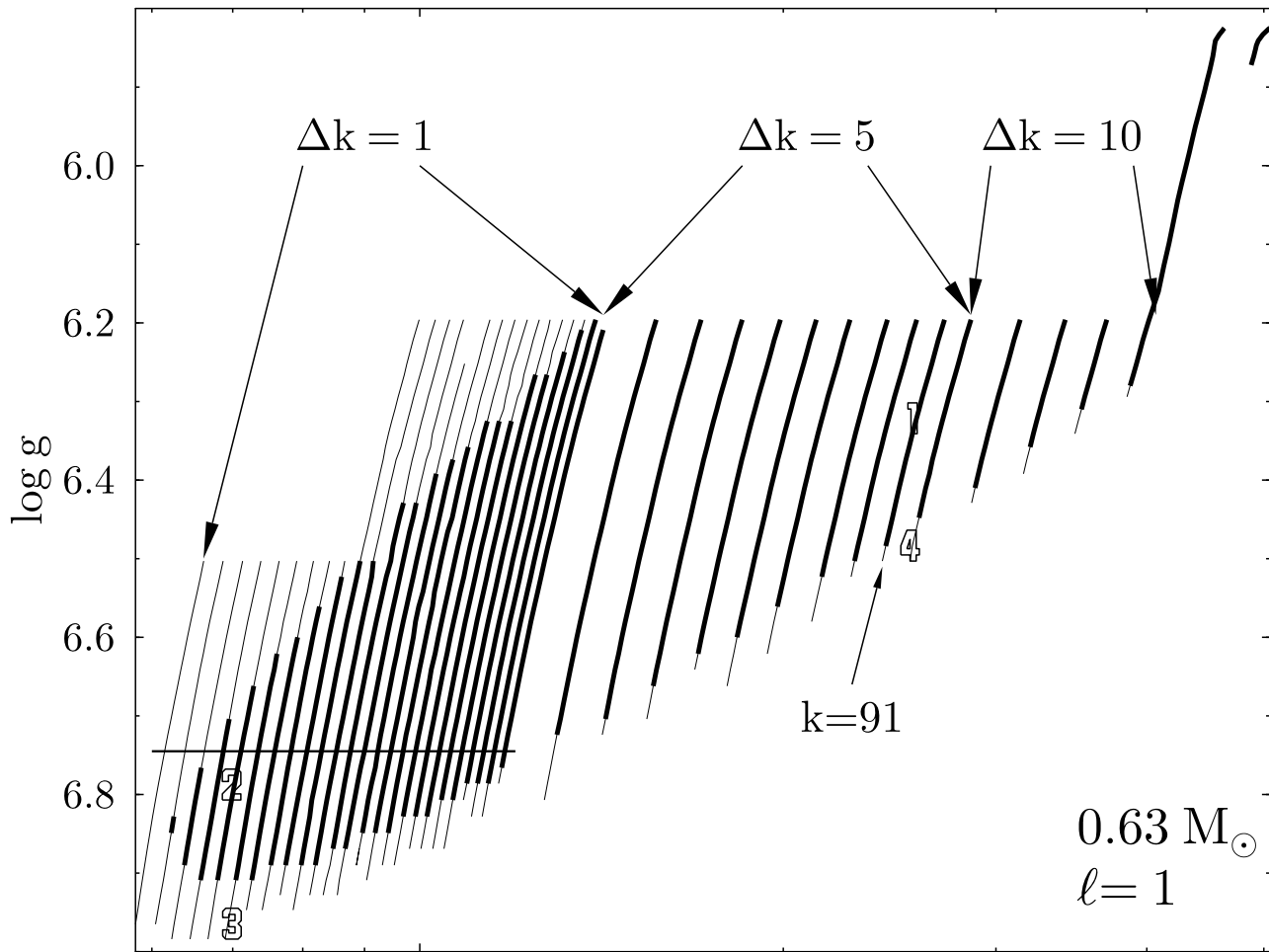
This article was processed by the author using Springer-Verlag TeX A&A macro package 1992.

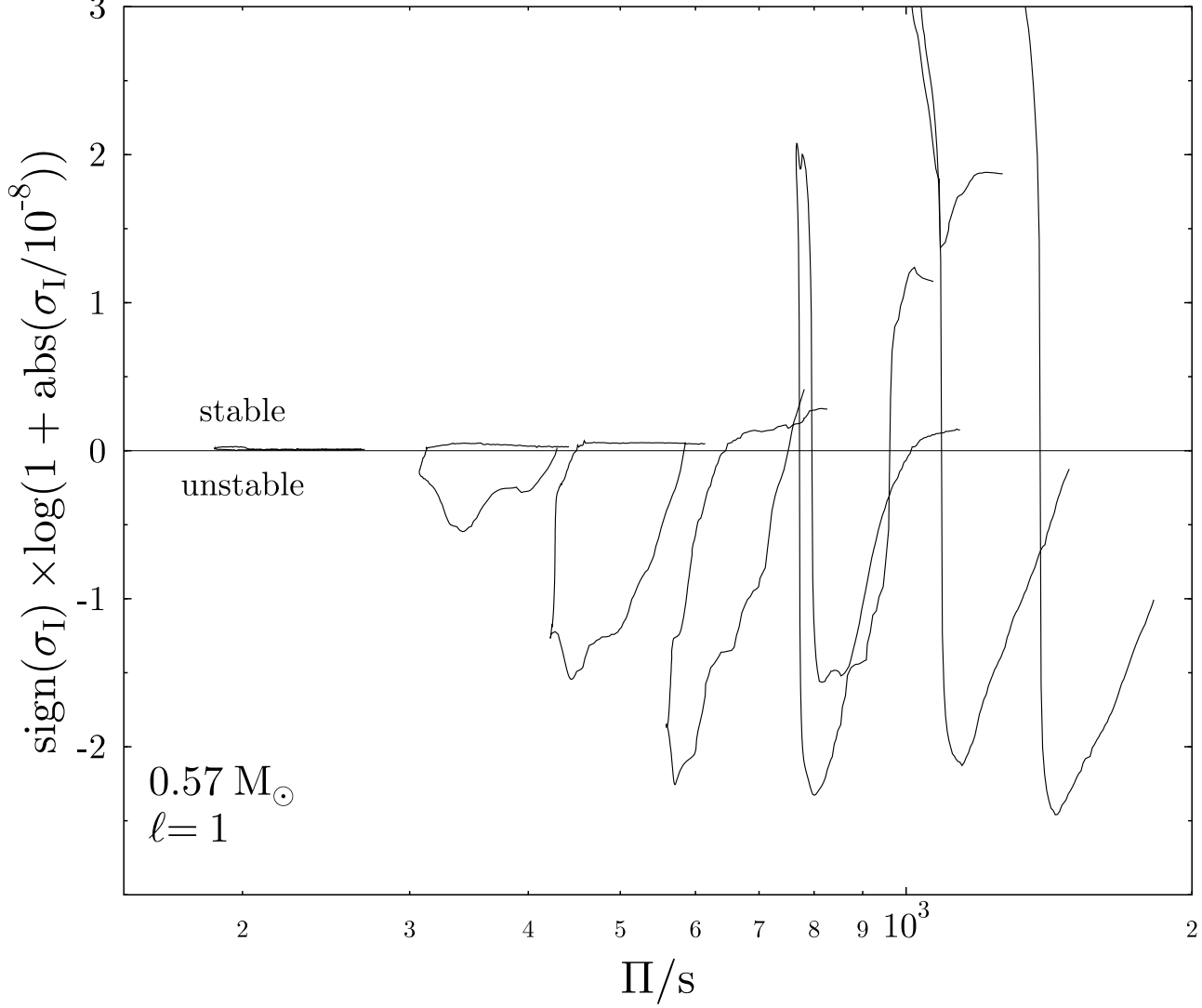
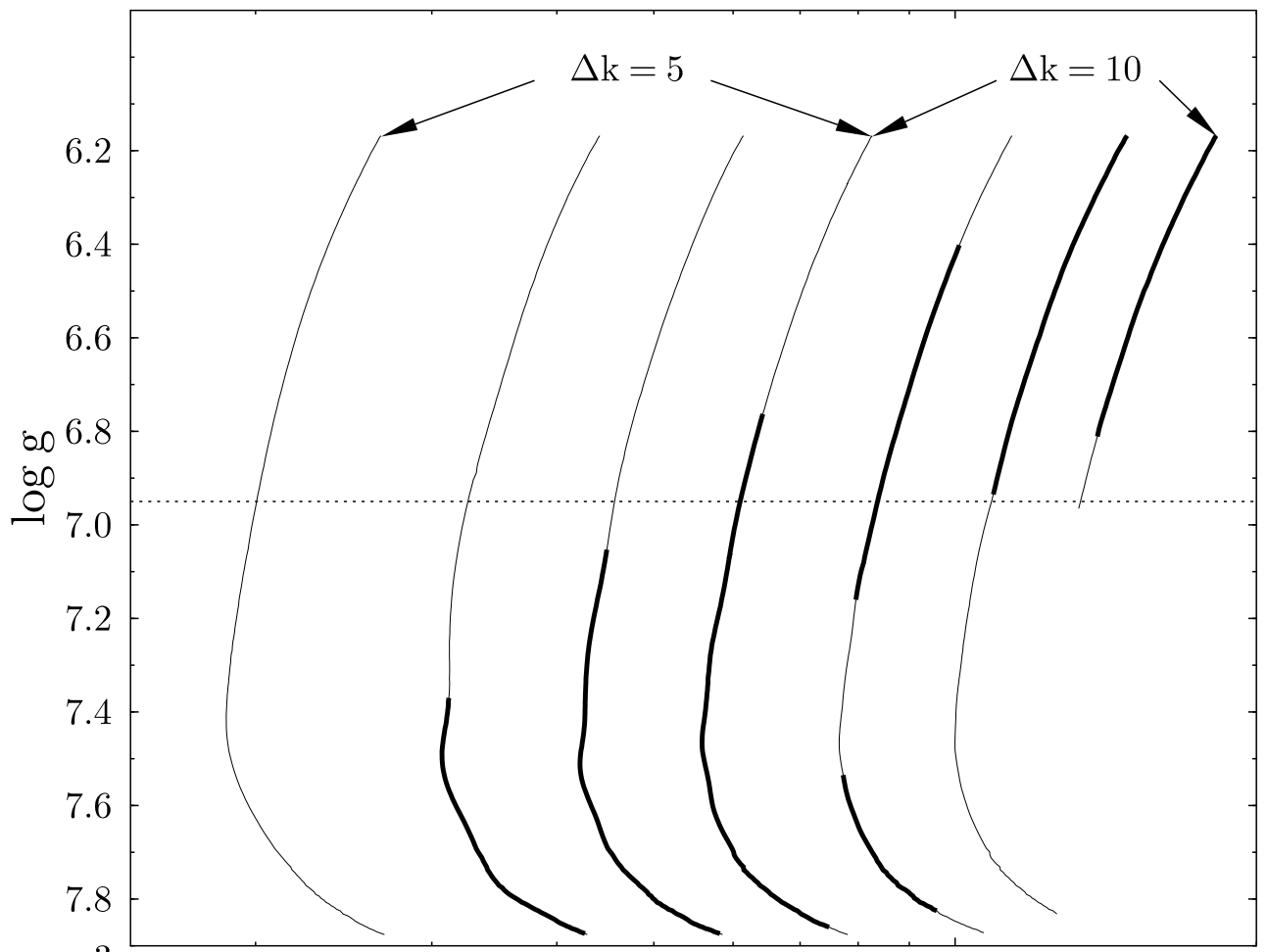


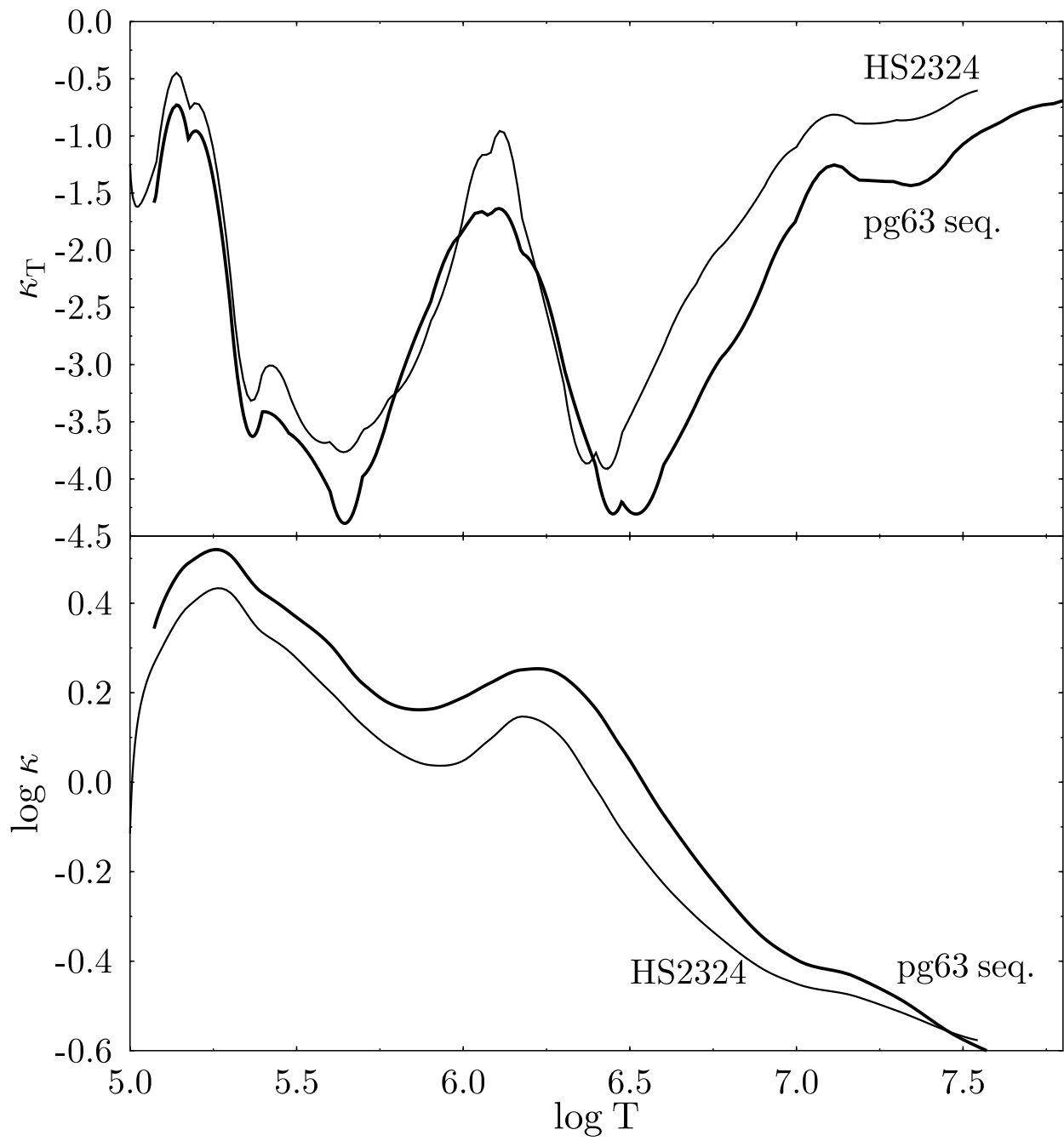






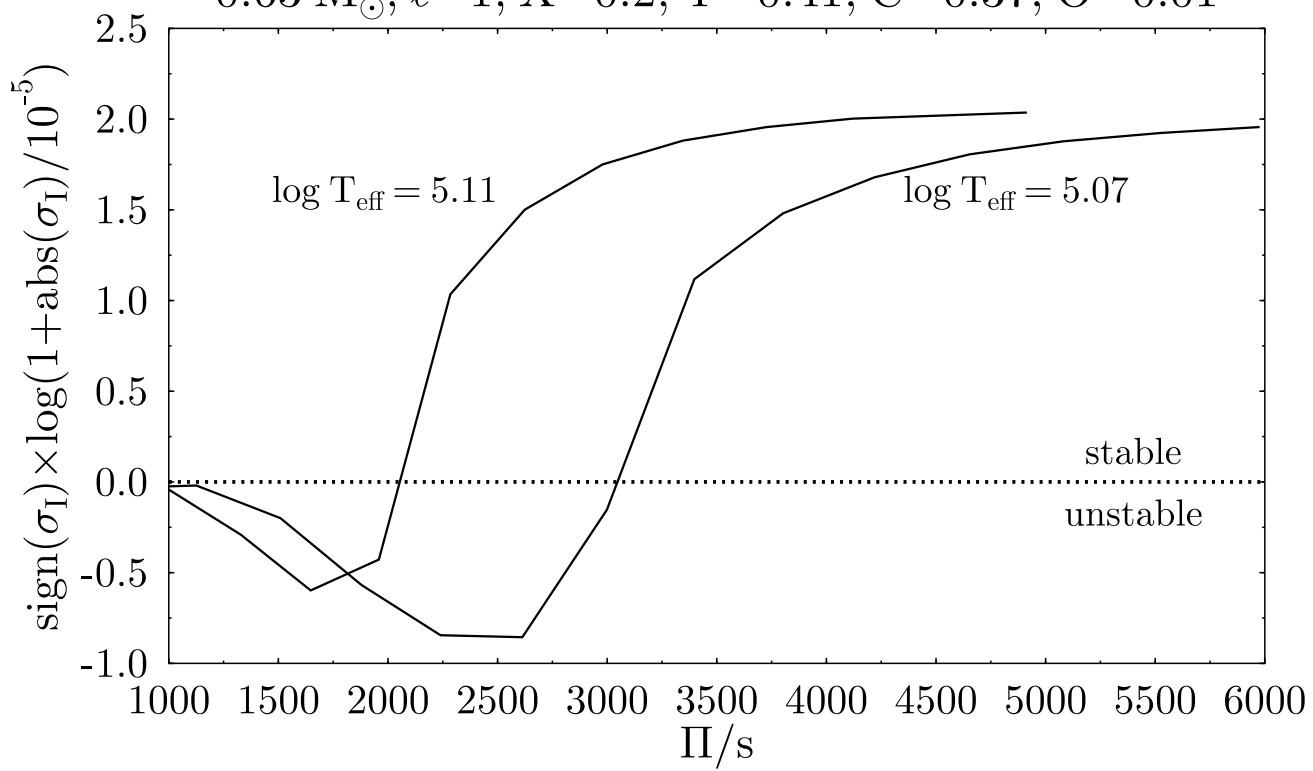


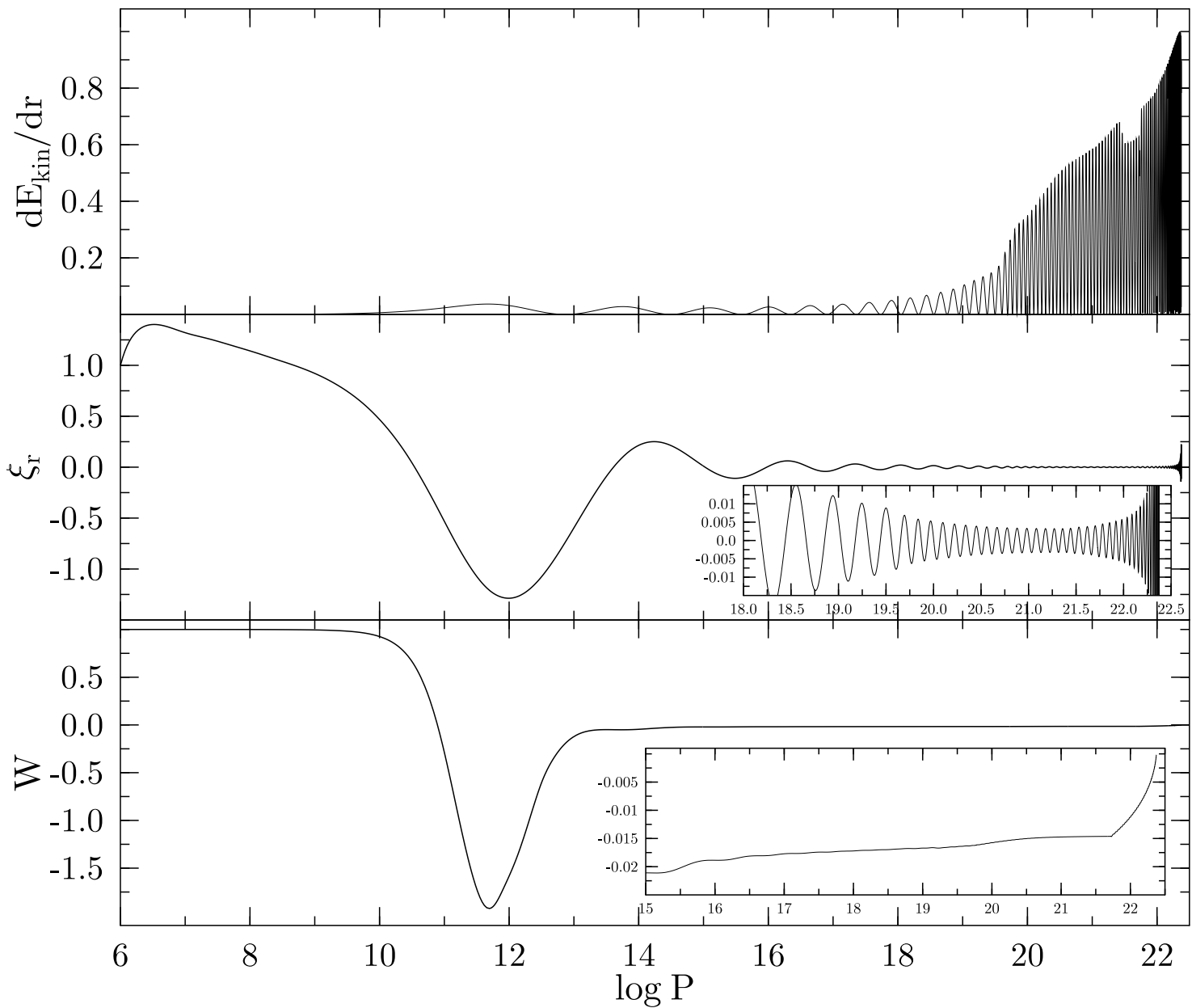


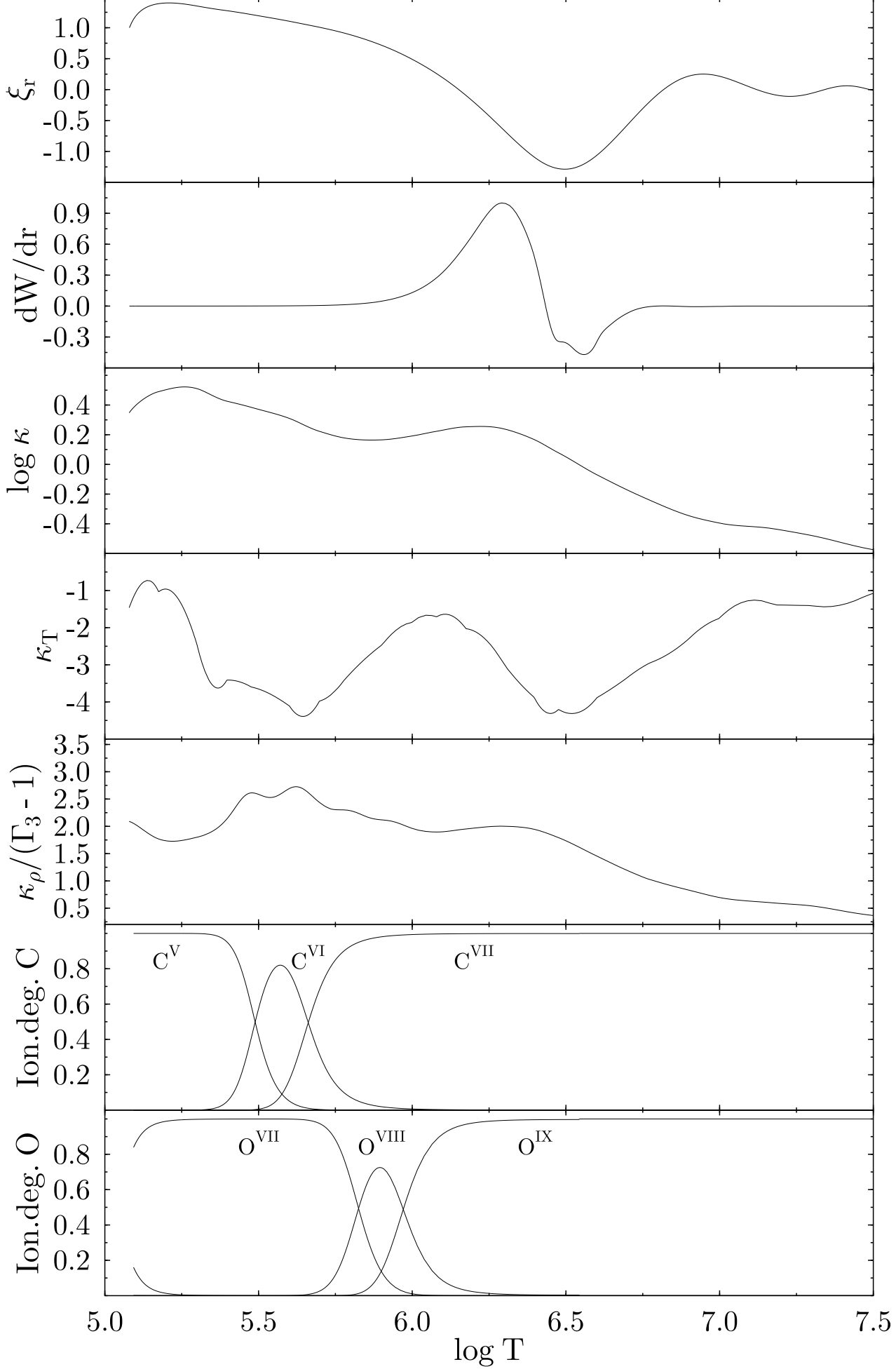




0.63 M<sub>⊙</sub>;  $\ell=1$ ; X=0.2, Y=0.41, C=0.37, O=0.01







$0.63 M_{\odot}, \log g = 6.745, \ell = 1$

